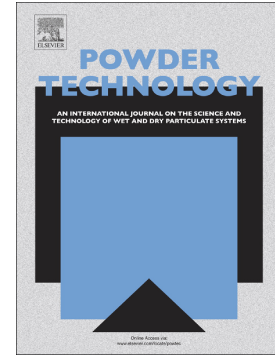


Journal Pre-proof

Investigation on nozzle zone agglomeration during spray drying using response surface methodology

Anneloes P. van Boven, Santiago M. Calderon Novoa, Reinhard Kohlus, Maarten A.I. Schutyser



PII: S0032-5910(23)00694-0

DOI: <https://doi.org/10.1016/j.powtec.2023.118910>

Reference: PTEC 118910

To appear in: *Powder Technology*

Received date: 13 June 2023

Revised date: 31 July 2023

Accepted date: 15 August 2023

Please cite this article as: A.P. van Boven, S.M. Calderon Novoa, R. Kohlus, et al., Investigation on nozzle zone agglomeration during spray drying using response surface methodology, *Powder Technology* (2023), <https://doi.org/10.1016/j.powtec.2023.118910>

This is a PDF file of an article that has undergone enhancements after acceptance, such as the addition of a cover page and metadata, and formatting for readability, but it is not yet the definitive version of record. This version will undergo additional copyediting, typesetting and review before it is published in its final form, but we are providing this version to give early visibility of the article. Please note that, during the production process, errors may be discovered which could affect the content, and all legal disclaimers that apply to the journal pertain.

© 2023 Published by Elsevier B.V.

Investigation on Nozzle Zone Agglomeration During Spray Drying Using Response Surface Methodology

Anneloes P. van Boven^{a,b}, Santiago M. Calderon Novoa^a, Reinhard Kohlus^b, Maarten A. I. Schutyser^{a*}

^aFood Process Engineering, Wageningen University & Research, P.O. Box 17, 6700 AA Wageningen, the Netherlands

^bUniversity of Hohenheim, Institute of Food Science and Biotechnology, Department of Process Engineering and Food Powders, Garbenstraße 25, 70599 Stuttgart, Germany

*Corresponding author: maarten.schutyser@wur.nl

Abstract

During spray drying, dry powder is circulated into the nozzle zone to force collisions, inducing agglomeration. This study systematically determined the effect of fine powder mass flowrate (varying from $7.1 \pm 1.2 - 15.9 \pm 0.5 \text{ kg}\cdot\text{h}^{-1}$), drying air temperature ($160 - 200 \text{ }^\circ\text{C}$), and drying air mass flowrate ($472.8 \pm 6.2 - 590.8 \pm 9.9 \text{ kg}\cdot\text{h}^{-1}$) on agglomerate size and morphology using a central-composite trial design. Agglomeration was quantified using an agglomeration index based on laser diffraction and by quantifying particle morphology using static image analysis. Response surface models were used to quantify factor effects. Increasing the fines mass flowrate had the largest positive effect on particle size enlargement and development of grape-like agglomerates. Increasing drying air temperature had a small negative effect on particle size enlargement and no significant effect on morphology. Increasing drying air mass flowrate had a small negative effect on particle size enlargement, but a positive effect on morphology. Finally, image analysis was found to be the preferred method to quantify the onset of agglomeration.

Key words: spray drying; agglomeration; response surface methodology; pilot-scale; nozzle zone; powder morphology

1. Introduction

Spray drying transforms liquid concentrates into powders to prolong shelf life and facilitate storage and transportation. A core benefit of this technique is that spray-dried powders have good functional properties like flowability, reconstitution behavior, bulk density, and mechanical stability, which are to a great extent determined by agglomeration during spray drying. During agglomeration, primary particles stick together to form agglomerates, which eliminates the presence of a large number of fine particles (<100 μm). Without proper agglomeration, powders often suffer from poor functional properties and may be even out-of-spec [1]. If the latter is the case, then a powder needs to be reworked or even discarded, contributing to food waste and thus incurring high energy use. Additionally, the presence of fine particles can pose process safety risks by their ability to cause dust explosions and can contribute to fine dust emission for which increasingly strict regulations are reinforced.

Although agglomeration is critical for powder production, optimization of this process during spray drying is done following a trial and error-based approach that has to be redone for every different dryer and product. On a larger scale, agglomeration is stimulated by the recycling of fines into the nozzle zone, for example in an industrial multi-stage spray dryer. Additionally, often multiple atomizers with overlapping spray clouds are used to stimulate droplet collisions. A better understanding on how to steer the agglomeration process would help to move away from this empirical approach to enable energy savings and obtain better powder quality control. Pilot-scale spray dryer set-ups that allow for controlled agglomeration are ideal to study the process of agglomeration [2]. Although researchers have investigated agglomeration, dosing fines in small spray dryer set-ups like the Büchi or the GEA Niro

Mobile Minor is not very realistic. Furthermore, having a rotary atomizer or a pressure nozzle, or a co-current or counter-current air pattern can have a major impact on the results.

At small pilot scale, researchers measured air properties in a GEA Niro Minor [3] to predict regions in the dryer where particles would be sticky (Gianfrancesco et al., 2009). They also extended this work with computational fluid dynamics (CFD) modeling of spray drying of maltodextrin solutions [5] and performed agglomeration trials with fines dosing [6]. They concluded that for successful agglomeration, the particle surface condition is more important than the collision rate. However, the experiments were conducted on a system with a rotary atomizer, and it would be interesting to test the findings with a pressure nozzle.

Williams et al. (2009) already compared the GEA Niro Minor to a bigger pilot scale spray dryer (evaporation capacity of $75 \text{ kg}\cdot\text{h}^{-1}$) and concluded that fines addition promotes agglomeration. Most favorable for agglomeration was a high feed flow rate with a low total solids content (TS) combined with a high flow of small fines. However, larger particles were obtained in situations with a high solids content of the feed and larger dry particles. Fröhlich et al. (2021) found that an increased feed TS created bigger agglomerates by shifting the collision outcomes from coalescence to agglomeration. However, Fröhlich et al. (2022) also found that an increase in TS decreases the relative fines mass flow, and that decreases the extent of agglomeration. In a multi-stage dryer, particles circulate until they are sufficiently large to reach the fluidized bed. Therefore, it is interesting to see what happens during one pass through the dryer, as increasing agglomeration in every pass limits the number of circulations, decreasing thermal damage. Additionally, researchers have tried to model the agglomeration process using CFD [10]. The complexity of the drying process causes a gap between simulation and reality, and experimental studies are needed to validate CFD models.

Conventional experimental approaches are often one factor at a time (OFAT). A major drawback of this is that a high number of experiments are required, which is expensive and time-intensive. Additionally, interactions between variables and their combined effects on the response are not taken into account [11]. Design of experiments (DoE) approaches can assist in explaining variation of output as a function of a set of changing conditions in an experiment. In this respect response surface methodologies (RSM) such as full factorial design and central composite design are useful as these allow investigating the effects of multiple varying process variables on an output variable [12,13].

Therefore, this study aimed to investigate how spray drying processing factors affect the onset of nozzle zone agglomeration using a response surface methodology. A face-centered, central composite trial design was used for agglomeration trials on a pilot-scale spray dryer. A single-stage spray dryer was used, during which dry, small powder particles (fines) were dosed in the nozzle zone to simulate one pass in an industrial multistage spray dryer. Input variables were the amount of fines dosed, drying air flow rate, and drying air inlet temperature, which were expected to affect both the collision probability and the sticking probability. The extent of agglomeration in the obtained powders was analyzed by calculating an agglomeration index (AI) based on the particle size distribution and by visual observations of particle morphology distributions using scanning electron microscopy (SEM) and a morphology analyser.

2. Materials and Methods

2.1. Materials

Maltodextrin DE 21 (MD21) was used as model system (Glucidex 21, Roquette Frères, France). The colorant ponceau red E124 was obtained from Natural Spices (the Netherlands). Regular tap water was used to prepared the feed.

2.1.1. Fines production

Feed with a TS of 40% (99.625 wt.% MD21 and 0.375 wt.% ponceau red) was prepared by dissolving the solids in hot tap water. The inlet drying air temperature was set at 160°C and the outlet temperature was 100°C. The feed was atomized using a SU2A two-fluid nozzle (Fluid Cap 2050, Air Cap 70) (Spraying Systems Co., USA) with an atomizing air pressure of 414 kPa. The powder that was collected was subsequently air classified to obtain a fraction with very small particle size. A Hosokawa Alpine Multi-mill system with an integrated air classifier (Hosokawa Micron B.V., the Netherlands) was used with a classifier rotor speed of 5000 rpm, and an inlet air flowrate of 40-55 m³h⁻¹ and a pressure drop across the classifier of 1.2-3.3 kPa. The fine fraction had a D(4,3) of 20.92 ± 0.24 μm and was used in further trials.

2.1.2. Experimental design and trial execution

Response surface methodology (RSM) was used for the pilot experiments using a three factor, five level () face-centered central composite design (CCD) (

Table 3). Runs were divided over three blocks or days. Within the blocks the runs were ordered on increasing temperature for practical reasons. The response factor was the agglomeration index (see 2.3.2). For every condition, a sample with and without fines dosing was run to correct for natural occurring agglomeration. A 40% w/w MD21 feed was prepared by adding the MD21 to hot tap water and stirring for at least 30 minutes until the feed became transparent. The atomization was kept constant throughout the trials at $21.2 \pm 0.4 \text{ kg}\cdot\text{h}^{-1}$ with a pressure of $40 \pm 2 \text{ bar}$ using a SIY78/SKY16 high pressure nozzle from Spraying Systems Co. (Wheaton, Illinois, USA), therefore the outlet temperature varied. The feed temperature at atomization varied between 29.5 and 34.7°C.

2.2. Spray drying

All spray drying experiments were performed on a DW-350 single stage pilot-scale spray dryer from Spray Dry Works (the Netherlands) (Figure 1) having a maximum drying capacity of $25 \text{ kg}\cdot\text{h}^{-1}$ and a drying chamber of 2 m in length and 1.5 m diameter. Ambient air was dehumidified using a Condair DA 1400 desiccant dryer (Switzerland) to a relative humidity of 5 % before an electrical heater heated it to the desired drying air inlet temperature (T_{in}). The DW-350 spray dryer has a Rotaswirl RC350 air distributor (Spray Dry Works, the Netherlands), with a perforated insert to reduce the air vortex. Outgoing air and powder were separated using a cyclone and the powder was collected through a rotary valve.

Fines were dosed with a screw, conveyed with ambient air using a small fan to the top of the spray dryer, and inserted concentrically to the nozzle at the inner inlet position (Figure 2).

2.3. Powder analysis

2.3.1. Moisture content

The powder moisture content (MC (%)) on total basis was determined in duplicate by oven drying at 105 °C overnight and calculated using Eq. (1).

$$MC = \frac{(m_{initial} - m_{final})}{m_{initial}} \cdot 100\% \quad (1)$$

where $m_{initial}$ (g) and m_{final} (g) are the sample masses before and after drying overnight, respectively.

2.3.2. Particle size analysis and agglomeration index

Particle size distributions (PSD) of the samples were determined in triplicate using laser diffraction with a Mastersizer 3000 (Malvern Panalytical, UK). An Aero S dry dispersion unit combined with a standard venturi dispenser was used to disperse the powder with a dispersion pressure of 3.5 bar.

To quantify the agglomeration caused by the fines dosing, the Agglomeration Index (AI) was calculated, as proposed by Williams (2007). The AI can be considered as a measure for the relative size enlargement occurring during one pass through a spray dryer. For this the mass fraction of primary feed MD21 particles ($x_{primary\ MD21}$ in $\text{g}\cdot\text{g}^{-1}$) in the final product was calculated using Eq. (2):

$$x_{primary\ MD21} = \frac{TS_{feed} \cdot \dot{m}_{feed}}{TS_{feed} \cdot \dot{m}_{feed} + \dot{m}_{fines} \cdot (100 - MC_{fines})} \quad (2)$$

where TS_{feed} ($\text{kg}\cdot\text{kg}^{-1}$) is the total solids content of the feed, \dot{m}_{feed} ($\text{kg}\cdot\text{h}^{-1}$) is the mass flowrate of the feed, \dot{m}_{fines} ($\text{kg}\cdot\text{h}^{-1}$) is the mass flowrate of dosed fines into the nozzle zone, and MC_{fines} (%) is the

moisture content of the dried fines. Subsequently, a theoretical PSD was calculated of the weighted average of the baseline PSD and the fines PSD based on the mass fractions using Eq. (3):

$$PSD_{theoretical} = x_{primary\ MD21} \cdot PSD_{baseline} + (1 - x_{primary\ MD21}) \cdot PSD_{fines} \quad (3)$$

where $PSD_{baseline}$ and PSD_{fines} ((%volume)($\log_{10}(\mu\text{m})$)⁻¹) are the PSDs of the samples without fines and of the fines, respectively. This calculated distribution indicates the distribution if no agglomeration would occur. This $PSD_{theoretical}$ was then subtracted from the distribution of the sample with dosed fines (Eq. (4)).

$$\Delta PSD = PSD_{sample} - PSD_{theoretical} \quad (4)$$

This ΔPSD , the difference distribution, is an indication to what extent smaller particles disappeared (negative areas) to form agglomerates (positive areas). However, to fairly compare samples with different mass flows of fines, the difference distribution should be normalized over the mass fraction of the spray in the product ($\frac{\Delta PSD}{x_{MD21}}$) and then integrated via a trapezoidal approximation using the average volume frequency for each histogram bin. Williams (2007) developed this procedure to censor the PSD of the fines from the sample distribution, and thus reduce the obscuration of fines in the PSDs. This is because the presence of more fines in the final powder will dilute the volume percentage of agglomerates in the sample. If this is not accounted for, a sample with high fines flowrate will not yield a high AI, even if it agglomerated extensively. The absolute area under the normalized curve is then divided by two and squared since the positive and negative areas of the difference distribution should be equal by definition (Eq. (5)).

$$AI = \left(\frac{1}{2} \int_0^{\infty} \frac{|\Delta PSD|}{x_{MD21}} d(\log_{10} d_{particle}) \right)^2 \approx \left(\frac{1}{2} \sum_{i=1}^j \frac{|\Delta PSD_i + \Delta PSD_{i-1}|}{2 \cdot x_{MD21}} \cdot \log_{10}(d_i - d_{i-1}) \right)^2 \quad (5)$$

In which ΔPSD_i ((% volume)($\log_{10}(\mu\text{m})$)⁻¹) is the volume weighted percentage of particles with diameters inside of a bin i (i.e. the volume of particles with diameters larger than d_{i-1} (μm) and smaller than d_i (μm)).

The agglomeration index assigns a quantitative value for samples with a larger number of formed agglomerates. Since the PSDs are volume-based distributions, the formation of large agglomerates will skew the difference distribution since larger particle diameters contribute more volume relative to smaller particles. Thus, the formation of larger agglomerates will enlarge the AI more drastically than the formation of relatively smaller agglomerates.

2.3.3. Particle shape analysis

The obtained powder was visually observed by using a JCM-7000 SEM (JEOL, Japan). Carbon tape was used to secure the samples on the aluminum sample holder. Loose powder was removed using pressurized air and the samples were then coated with gold using a JEOL Smart-Coater (JEOL, Japan). The images were taken at an acceleration voltage of 5 kV.

Particle morphology of the powders was analyzed with a Malvern Morphologi 4 (Malvern, UK). For each sample, 19 mm³ of powder was dispersed onto the glass plate and individual particles were photographed and using image analysis descriptive shape factors such as HS circularity, elongation and solidity were determined. For each sample >30,000 particles were analyzed. Using the shape factors, the particles were divided into primary, partially coalesced and agglomerated particles (

Table 2). Particles that did not fall within these classes, were classified as 'other' (N_o).

2.4. Response surface model development

A response-surface model was fit relating the AI values to the input variables of the CCD experiments using a linear least-squares regression algorithm. However, for the drying air flow rate there were large fluctuations because the flow rate at a given capacity depends on the air density, which changes with temperature. Therefore, the actual factor levels were calculated (Eq.(6) Table A. 1) and used instead of the expected levels in the response surface model.

$$x_i = \frac{(X_i - X_{i,0})}{\Delta X_i}; \Delta X_i = \frac{(X_{i,1} - X_{i,-1})}{2}; i = 1, 2, 3 \quad (6)$$

where x_i is the coded factor of the natural variable X_i , where i is the subscript indicating the factor. The drying air temperature was x_1 , the fines mass flowrate was x_2 , and the drying air mass flowrate was x_3 . $X_{i,0}$ represents the value of the process variable at its midpoint: $X_{1,0} = 180^\circ\text{C}$; $X_{2,0} = 10.9 \text{ kg} \cdot \text{hr}^{-1}$; $X_{3,0} = 541.3 \text{ kg} \cdot \text{hr}^{-1}$. $\Delta X_{i,1}$ and $\Delta X_{i,-1}$ are the process variables at the low and high factorial levels. ΔX_i is the average difference in the level X_i as it is increased by 1 unit of x_i : $\Delta X_1 = 12^\circ\text{C}$; $\Delta X_2 = 3.19 \text{ kg} \cdot \text{hr}^{-1}$; $\Delta X_3 = 36.7 \text{ kg} \cdot \text{hr}^{-1}$. The coded values of all the process conditions were then used to fit the RSM models.

Firstly, a second-order model was fit to the AI using the *rsm* package (version 2.10.3) for R in RStudio (version 4.2.2). This model fits a second-order model with pure quadratic terms, two-way interaction terms, and linear terms (Eq. (7)).

$$AI = \beta_0 + \beta_1 x_1 + \beta_2 x_2 + \beta_3 x_3 + \beta_{12} x_1 x_2 + \beta_{13} x_1 x_3 + \beta_{23} x_2 x_3 + \beta_{11} x_1^2 + \beta_{22} x_2^2 + \beta_{33} x_3^2 \quad (7)$$

Where x_1, x_2, x_3 are the coded variables for drying air temperature, fines mass flowrate, and drying air flowrate respectively, β_0 is the intercept (fitted value of AI when $(x_1, x_2, x_3) = (0,0,0)$), $\beta_1, \beta_2, \beta_3$ are the

coefficients for the linear terms, $\beta_{12}, \beta_{13}, \beta_{23}$ the coefficients for the two-way interaction terms between coded variables and $\beta_{11}, \beta_{22}, \beta_{33}$ the coefficients for the pure quadratic terms.

Next, the model was refined by following stepwise regression. Here, terms are removed (i.e. interaction terms or quadratic terms) and analysis of variance (ANOVA) is computed to obtain the corrected Akaike Information Criteria (AIC). Via this procedure the model with the lowest AIC was found, describing the data, containing only significant terms, and lowest residuals. The model adequacy was checked by calculating the R^2 and adjusted- R^2 values. The same procedure was repeated to fit the model to the N_{agg} .

3. Results and Discussion

3.1. Response Surface Model Development

The AI values were calculated (

Table 3) and fit to the second-order model presented in Eq. (7). From the model comparison, the model that described the data with the lowest AIC was derived (Eq. (8)), which also contained a blocking factor (D) distinguishing the days on which the experiments were performed. The model parameter estimates, standard error and significance of each term were determined (Table A. 2). Factors with a p value ($Pr(>|t|)$) below 0.2 indicates significance. However, a compromise was made by leaving in terms with significance up to 0.22 since removing them made the model less accurate. This model had an R^2 of 0.90 and an adjusted- R^2 of 0.84. Using the derived model, response surfaces and contour plots for the AI were created to assess the effect of the processing conditions (Figure 3).

The response surfaces, contour plots and parameter estimates show that increasing the x_1 (T_{in}) and x_3 (mass flow air) had a negative effect on the extent of agglomeration, while increasing x_2 (mass flow fines) had a positive effect on the extent of agglomeration. The effect of the flowrate of fines and drying air (x_2, x_3) on the AI was larger than of the drying air temperature (x_1), which can also be concluded from the estimated parameter values (Eq. (8)).

The obtained AI values represent the agglomeration that occurs during one pass through the nozzle zone and are of the same order of magnitude as AI values found for a one-pass agglomeration during spray drying by Williams et al. (2009). The AI values found in that study were slightly lower than in this study (0.008-0.127 versus 0.037-0.189). Those values were obtained at lower fines-to-spray (F:S) ratios (0.15-0.4 versus 0.824-1.841). This is due to the nozzle zone setup of the dryer used in that work. The dryer had a fines inlet with three spray nozzles positioned evenly around the fines inlet and directed towards the center of the drier. This setup forces collisions more than the concentric fines curtain used for the CCD trials (Figure 2). In industrial multi-stage dryers, particles are recycled until they are sufficiently large to overcome the upwards flow and reach the fluid bed [9]. AI values here thus represent the onset of nozzle zone agglomeration, and will be larger when multi-stage dryers are used.

$$AI = 0.07173 + 0.01222D_2 - 0.02041D_3 + 0.01440D_4 - 0.00648x_1 + 0.03689x_2 - 0.01357x_3 - 0.00779x_1x_2 + 0.00712x_2^2 + 0.00739x_3^2 \quad (8)$$

3.2. Effect of processing conditions on AI

All three variables affected the AI. The AI was found to decrease as the drying air temperature (x_1) increased. This may be related to the effect of temperature on the drying rate, which changes the sticking probability. At higher temperatures, droplets dry more quickly and become more surface-dry and less sticky before colliding with incoming fines, resulting in reduced adhesion. These findings match earlier findings from Both et al. (2020), who observed a faster surface-dry skin forming around the droplets at higher air inlet temperatures, causing a lack of adhesion upon collision. Additionally, the authors found a higher fraction of particles that were likely to be agglomerates at lower temperatures. The fines flowrate (x_2) increases agglomeration by increasing the collision probability. Introducing more fine particles under the same drying conditions increases the likelihood of a collision. This is in line with findings from Fröhlich et al. (2023) and Williams et al. (2009). A higher drying air flowrate (x_3) was found to decrease the AI. The effect of the drying air flowrate is two-fold. First, it affects the sticking probability as a higher drying air mass flowrate increases the drying rate. As with temperature, an increased drying rate causes a drying droplet to be surface-dry faster. Second, it affects the collision probability. Using less drying air decreases the turbulence in the nozzle zone. Turbulence can disrupt the fines stream entering the drying chamber and spread the particles quickly, which decreases the particle concentration in the interaction zone, lowering the collision probability. Hence, a lower drying air flowrate is beneficial for agglomeration.

Since the drying air temperature and flowrate both affect the drying rate, it is interesting to study the relationship between drying rate and agglomeration more closely. The effects can be combined by calculating the thermal energy supplied by the drying air per kg feed supplied (\dot{Q}_{da} (kJ·kg⁻¹ total basis),

Eq. (9) in which \dot{m}_{da} ($\text{kg}\cdot\text{h}^{-1}$) is the mass flowrate of dry air supplied into the dryer, $C_{p,a}$ & $C_{p,wv}$ ($\text{kJ}\cdot\text{kg}^{-1}$) are the specific heat capacities of air and water vapor, AH ($\text{kg}\cdot\text{kg}^{-1}$) is the absolute humidity of the inlet air, T_{in} (K) is the inlet temperature of the drying air, Δh_v ($\text{kJ}\cdot\text{kg}^{-1}\cdot\text{K}^{-1}$) is the enthalpy of vaporization for water, and \dot{m}_{feed} is the mass flowrate of the feed on total basis ($\text{kg}\cdot\text{h}^{-1}$). The AI decreases for increasing supplied \dot{Q}_{da} (Figure 4), confirming that a higher drying rate reduces agglomeration. The AI drops less upon increasing \dot{Q}_{da} for lower fines flowrates, which can be linked to the interaction term $\beta_{12}x_1x_2$ from Eq. (5). For higher fines flowrates, this meant that the AI dropped more drastically because more fines were bouncing off and not contributing to particle enlargement of the sprayed droplets. The spread in AI values within each class of \dot{m}_{fines} is partly caused by the different days on which the experiments were carried out, which has been taken into account in the model by the introduction of blocking factor D (eq. (8)).

$$\dot{Q}_{da} = \frac{\dot{m}_{da}}{\dot{m}_{feed}} \cdot \left((C_{p,a} + C_{p,wv} \cdot AH) \cdot T_{in} + AH \cdot \Delta h_v \right) \quad (9)$$

When a dry fine particle collides with a completely wet droplet they coalesce and the dry particle is fully absorbed. The volume of such droplets after collision hardly increases and this type of collision is therefore undesired. During drying, the droplet changes from wet to sticky to dry, and the collision outcomes shift from coalescence, to sticking to bouncing. It was therefore expected that there would be an optimum drying rate. However, no drying rate optimum was found to be significant within the experimental range. It seems that more drying leads to less agglomeration, indicating a shift from sticking to bouncing. A drying rate optimum could be suspected from the curvature when plotting drying air flowrate versus temperature (Figure 3), where there was some curvature leading to an increase in AI as x_1 was varied from $-\alpha$ to 0, and then a decrease as x_1 was varied from 0 to α . However, since the quadratic term for x_1 was not significant, it is not possible to conclude if this optimum of the drying rate

exists, or if it is just the curvature of the interaction term $\beta_{12}x_1x_2$. Moreover, the effect of temperature was small, if significant at all.

3.3. Predicting power of RSM

To test the predicting power of the RSM, during block 4 a test point ($\alpha, \alpha, -\alpha$) was included to see how well the model could predict the AI for conditions outside of the experimental range. The model was capable of predicting the AI up to a 95% confidence interval (Figure 5). In terms of agglomeration performance, this condition had a larger AI (0.189) than the CCD points, indicating that operating at a high fines flowrate and low massflow of drying air leads to more agglomeration. This verifies the trends uncovered by the model that a high fines flowrate and low massflow of drying air are beneficial for agglomeration. Possibly, with a low temperature ($-\alpha, \alpha, -\alpha$) an even higher AI would have been measured, ($AI_{predicted} = 0.250$), but the effect is assumed to be smaller than that of the other factors. There is less deviation from the trend in Figure 5 than in Figure 4 because the model incorporates the blocking factor D to correct for the spread caused by the different days on which the experiments were carried out.

3.4. Effect of processing conditions on particle morphology

Although the AI shows that particle size enlargement occurred, it does not indicate whether larger particles were formed by (partial) coalescence or agglomeration. However, different structures have distinct functional properties, leading to a preference for, for example, a grape structure. In literature, researchers have investigated where in a spray dryer particles may agglomerate or coalesce [17–19], but experimental results are lacking. Comparing the types of structures between experimentally produced samples can give some indications of how drying conditions affect the collision outcomes. Morphology analysis results (Figure 6) are presented without comparison to the powders without fines addition. Therefore, differences between samples are due to changes in natural agglomeration of the droplet-

droplet collisions *and* forced agglomeration of droplet-fines collisions. The number of particles that could not be classified (N_o), was low.

A model was fitted to explain the influence of the parameters on the fraction of agglomerates. Since the six-fold repetition of the center point yields different N_f -values, a model including a blocking factor was fitted (Eq.(10)). The model fit was less good than that of the AI model, as this model has an adjusted- R^2 of 0.622 and the AI model of 0.8391. The parameter estimates indicate that the fines mass flowrate had the biggest effect on the N_{agg} and that drying air temperature was not a significant factor in explaining the difference in N_{agg} .

$$N_{agg} = 0.07673 + 0.03122D_2 + 0.06796D_3 - 0.01378D_4 + 0.01091x_2 + 0.00821x_3 \quad (10)$$

The number of agglomerated particles (N_{agg}) increases for increasing fines flowrates (x_2). This is in line with the AI, which is higher for those conditions. When no agglomeration would have occurred during fines dosing, the number of primary particles (N_{p_1}) should have increased drastically for higher fines dosing rates due to the presence of more unagglomerated fines. The effect of the fines flowrate on the morphology of the samples is not as strong as on the AI. This can be explained since the morphology analyses were not compared to the "no-fines" condition, it is difficult to distinguish if the changes occur by increasing natural or forced agglomeration. The main conclusion that can be drawn is that adding fines results in the formation of more agglomerate clusters, which could be expected.

However, within each fines dosing rate, there is also variation, meaning that the drying air temperature and mass flow also affected the obtained morphologies. The drying air flowrate (x_3) increased N_{agg} , which is opposite to its effect on AI. It is hypothesized that the increase in the air flowrate affected the smaller particles in the nozzle zone more than the larger ones. This makes physical sense as smaller particles have less inertia (Williams, 2007). This could have led to more collisions between fines and smaller spray particles, forming rather small agglomerates. This outcome could explain a decrease in AI

and an increase in N_{agg} because the agglomerate subclass did not filter for size and can include small grape agglomerates. This result must be taken with caution as the smaller the particles are, the lower the relative resolution of the particles. Hence, the shape parameters calculated from the projection of a small agglomerate do not have the same accuracy as a large agglomerate. However, this trend describes a trade-off between particle enlargement (AI) and particle morphology (N_{agg}) since increasing the air flowrate decreases AI while increasing N_{agg} .

Again, the effects of drying air temperature and drying air flowrate on morphology can be combined by calculating the \dot{Q}_{da} . Increasing the thermal energy supplied by drying air led to a decreasing trend in N_{pc} at the expense of an increase in N_{pp} . For a given fines flowrate, increasing the thermal energy seems to have reduced the partially coalesced fraction while keeping the agglomerate fraction unaffected (Figure 7). Partial coalescence is only possible if the particles are still liquid enough so that they can penetrate before the larger particle dries. The results indicate that when \dot{Q}_{da} was increased in the nozzle zone, the droplets dried more rapidly, reducing the incidence of coalescence while relatively increasing the incidence of agglomeration (particles penetrated less than 50% of their diameter). Moreover, increasing \dot{Q}_{da} led to the formation of more primary particles, which is most probably related to the over-drying of droplets resulting in surface-dry skins [15,20]. These results point to lower drying rates yielding a size enlargement that might not be as desired as higher drying rates as partial coalesced particles do not bring the functional benefits that grape-type agglomerates do. However, these results only apply for a single pass through the nozzle zone and may change when the size of the dry particles changes upon circulating through the nozzle zone more times.

3.5. Comparing nozzle zone agglomeration by microscopy

Because the AI and the N_{agg} give contradicting results, the samples were also visually compared using SEM (Figure 8). The samples that seem to be more agglomerated, have a higher N_{agg} value, but lower AI values. It is important to bear in mind that the AI is a measure for particle volume increase upon fines addition. Samples with higher AI values do not necessarily have a larger particle size, but they have grown the most compared to the condition without fines addition. The AI is based on measurements with laser diffraction, a method based on the principle that particles of different sizes scatter the light differently. The particle size is then presented as the diameter of a sphere with the same volume [21]. However, the particles are often largely spherical, but with a fine particle attached to them (Figure 8). The AI is based on volume increase, but the adherence of a fine to a coarse particle hardly affects its total volume. With the morphological classes from the image analysis, these small attached particles are better taken into account. This means that the morphological analyses represent the samples better, making image analysis the preferred method to compare the agglomeration between the samples. This applies to the investigation of the onset of nozzle zone agglomeration. To investigate the agglomeration of powders produced in a multi-stage spray dryer, the AI may be much more indicative than here. This is because the powder in that case would consist only of agglomerates and not a mixture of primary particles, partially coalesced particles, and agglomerates.

4. Conclusion

The effect of drying air temperature ($160 - 200$ °C), fines flowrate ($7.1 \pm 1.2 - 15.9 \pm 0.5$ kg·h⁻¹), and drying air flowrate ($472.8 \pm 6.2 - 590.8 \pm 9.9$ kg·h⁻¹) on nozzle zone agglomeration was systematically investigated using response surface modeling. The results showed that fitting a response-surface model to a designed experiment provided a way to statistically study a complex system with relative ease and efficiency. The experimental design consisted of a central-composite design with eight factorial

treatments, twelve axial treatments (six treatments in duplicate), and six center treatments. To compare size enlargement due to fines supplementation across treatments, an agglomeration index (AI) was applied. To compare morphological differences across treatments, static image analysis methods were applied to separate the particles into subclasses.

It was found that conditions that favored size enlargement of powder particles were those with low drying air temperatures and flowrates, and high fines supplementation flowrates. Regarding morphology, an increase in fines flowrate and air flowrate led to more grape-like cluster agglomerates being formed. From these three factors, the fines supplementation flowrate was the most significant in impacting both the size enlargement as well as the development of grape-like clusters.

It was hypothesized that conditions that increased the collision frequency in the nozzle zone (i.e. increase in fines mass flowrate, decrease in air flowrate) would lead to higher extent of agglomeration. This was confirmed when analyzing the size enlargement due to fines supplementation. Interestingly, increasing the air flowrate negatively affected size enlargement while improving agglomerate quality. An improvement in agglomerate quality consisted of an increase in the fraction of non-circular, irregularly-shaped grape clusters. Considering the limitations of laser diffraction, which form the basis of the AI, division into morphological classes based on image analysis is the preferred method to compare the onset of agglomeration between samples.

It was hypothesized that increasing the drying air temperature would show a maximum positive effect on agglomeration outcomes up to a critical value as the droplet surface changed from wet to sticky. After this critical value, the droplet surface would become too dry, causing more fines to bounce off it instead of agglomerating. The obtained results were not conclusive when analyzing the drying air temperature, as the effect of temperature on AI was small and not significant on N_{agg} . However, considering the thermal energy provided by the drying air (Q_{da}), samples that were exposed to higher drying rates

(higher Q_{da} values) were systematically less agglomerated (lower AI) and had higher fractions of primary, non-agglomerated particles (higher N_{pp}). For this study, the feed consisted of maltodextrin DE21 only, and the dosed fines consisted of maltodextrin DE21 with a small fraction of colorant. Although found trends can likely be extrapolated to other compounds, the exact values might differ per compound as they have a different T_g and viscosity and thereby have different stickiness regimes.

5. Acknowledgments

This work is an Institute for Sustainable Process Technology (ISPT) project, i.e. StAggloP (Project number: DR-50-15). Partners in this project are Corbion, Danone, DSM, FrieslandCampina, University of Hohenheim, Wageningen University & Research, and ISPT. This project is co-funded with subsidy from the Topsector Energy by the Dutch Ministry of Economic Affairs and Climate Policy. We would like to thank Jos Sewalt for his assistance during spray drying trials and Maurice Strubel for the SEM images and David Hollestelle and Jewe Schröder for their support in setting up the spray dryer configuration.

6. Author CRediT statements

- Anneloes van Boven: Conceptualization, investigation, methodology, writing – original draft
- Santiago Calderon Novoa: Investigation, methodology, formal analysis, writing – original draft
- Reinhard Kohlus: Conceptualization, funding acquisition, supervision, writing – review & editing
- Maarten Schutyser: Conceptualization, funding acquisition, supervision, writing – review & editing

7. References

- [1] H. Kessler, Food and Bio Process Engineering - Dairy Technology, fifth edit, Publishing House A. Kessler, München, 2002.
- [2] N.M. Eijkelboom, A.P. van Boven, I. Siemons, P.F.C. Wilms, R.M. Boom, R. Kohlus, M.A.I. Schutyser, Particle structure development during spray drying from a single droplet to pilot-scale perspective, *J Food Eng.* 337 (2023) 111222. <https://doi.org/10.1016/J.JFOODENG.2022.111222>.
- [3] A. Gianfrancesco, C. Turchiuli, E. Dumoulin, Powder agglomeration during the spray-drying process: Measurements of air properties, *Dairy Sci Technol.* 88 (2008) 52–64. <https://doi.org/10.1051/dst:2007008>.
- [4] A. Gianfrancesco, C. Turchiuli, E. Dumoulin, S. Palzer, Prediction of Powder Stickiness along Spray Drying Process in Relation to Agglomeration, *Part Sci and Technol.* 27 (2009) 415–427. <https://doi.org/10.1080/02726350903279987>.
- [5] A. Gianfrancesco, C. Turchiuli, D. Flich, E. Dumoulin, CFD Modeling and Simulation of Maltodextrin Solutions Spray Drying to Control Stickiness, *Food Bioproc Tech.* 3 (2010) 946–955. <https://doi.org/10.1007/s11947-010-0352-2>.
- [6] C. Turchiuli, A. Gianfrancesco, S. Palzer, E. Dumoulin, Evolution of particle properties during spray drying in relation with stickiness and agglomeration control, *Powder Technol.* 208 (2011) 433–440. <https://doi.org/10.1016/j.powtec.2010.08.040>.
- [7] A.M. Williams, J.R. Jones, A.H.J. Paterson, D.L. Pearce, Effect of fines on agglomeration in spray dryers: An experimental study, *Int J Food Eng.* 5 (2009). <https://doi.org/10.2202/1556-3758.1635>.

- [8] J.A. Fröhlich, T.V. Raiber, J. Hinrichs, R. Kohlus, Nozzle zone agglomeration in spray dryers : Influence of total solid content on agglomerate properties, *Powder Technol.* 390 (2021) 292–302. <https://doi.org/10.1016/j.powtec.2021.05.094>.
- [9] J.A. Fröhlich, M. Spiess, J. Hinrichs, R. Kohlus, Nozzle zone agglomeration in spray dryers: Process dependency of the fines mass flow and its importance for agglomerate formation, *Dry Technol.* (2022) 1–13. <https://doi.org/10.1080/07373937.2022.2111439>.
- [10] R.E.M. Verdurmen, G. Van Houwelingen, M. Gungsing, M. Verschueren, J. Straatsma, Agglomeration in spray drying installations (the EDECAD project): Stickiness measurements and simulation results, *Dry Technol.* 24 (2006) 721–726. <https://doi.org/10.1080/07373930600684973>.
- [11] N. Malekjani, S.M. Jafari, Food Process Modeling and Optimization by Response Surface Methodology (RSM), in: *Mathematical and Statistical Applications in Food Engineering*, CRC Press, 2020: pp. 181–203. <https://doi.org/10.1201/9780429436963-13>.
- [12] M. Homayoonfal, N. Malekjani, Y. Baghbali, E. Ansarifard, S. Hedayati, S.M. Jafari, Optimization of spray drying process parameters for the food bioactive ingredients, *Crit Rev Food Sci Nutr.* (2022). <https://doi.org/10.1080/10403398.2022.2156976>.
- [13] D. Montgomery, *Design and Analysis of Experiments*, 9th ed., Wiley, 2017. [https://books.google.nl/books?hl=nl&lr=&id=Py7bDgAAQBAJ&oi=fnd&pg=PA1&dq=Montgomery,+D.+C.+Design+and+Analysis+of+Experiments,+10th+Edition,+Wiley.+Wiley+1%E2%80%93682+\(2020\)&ots=X7w2q2SMZ3&sig=1RIPMWBhYhNJ4hNfEkZnWELCuWU#v=onepage&q&f=false](https://books.google.nl/books?hl=nl&lr=&id=Py7bDgAAQBAJ&oi=fnd&pg=PA1&dq=Montgomery,+D.+C.+Design+and+Analysis+of+Experiments,+10th+Edition,+Wiley.+Wiley+1%E2%80%93682+(2020)&ots=X7w2q2SMZ3&sig=1RIPMWBhYhNJ4hNfEkZnWELCuWU#v=onepage&q&f=false).
- [14] A.M. Williams, *Instant milk powder production: determining the extent of agglomeration*, PhD, Massey University, Palmerston North, 2007.

- [15] E.M. Both, R.M. Boom, M.A.I. Schutyser, Particle morphology and powder properties during spray drying of maltodextrin and whey protein mixtures, *Powder Technol.* 363 (2020) 519–524.
<https://doi.org/10.1016/j.powtec.2020.01.001>.
- [16] J.A. Fröhlich, N.A. Ruprecht, R. Kohlus, Nozzle zone agglomeration in spray dryers: Determination of the agglomeration efficiency in the fines return by means of agglomerate properties and residence time distribution, *Dry Technol.* (2023). <https://doi.org/10.1080/07373937.2023.2203224>.
- [17] H. Jubaer, J. Xiao, X.D. Chen, C. Selomulya, M.W. Woo, Identification of regions in a spray dryer susceptible to forced agglomeration by CFD simulations, *Powder Technol.* 346 (2019) 23–37.
<https://doi.org/10.1016/J.POWTEC.2019.01.088>.
- [18] L. Malafronte, L. Ahrné, F. Innings, A. Jongsma, A. Rasmussen, Prediction of regions of coalescence and agglomeration along a spray dryer—application to skim milk powder, *Chem Eng Res Des.* 104 (2015) 703–712. <https://doi.org/10.1016/J.CHERD.2015.10.011>.
- [19] F. Hussain, M. Jaskulski, M. Piatkowski, E. Tsotsas, CFD simulation of agglomeration and coalescence in spray dryer, *Chem Eng Sci.* 247 (2022). <https://doi.org/10.1016/J.CES.2021.117064>.
- [20] R.E.M. Verdurmen, P. Menn, J. Ritzert, S. Blei, G.C.S. Nhumaio, T.S. Sørensen, M. Günsing, J. Straatsma, M. Verschuren, M. Sibeijn, G. Schulte, U. Fritsching, K. Bauckhage, C. Tropea, M. Sommerfeld, A.P. Watkins, A.J. Yule, H. Schønfeltdt, S. Sørensen, Simulation of Agglomeration in Spray Drying Installations: The EDECAD Project, *Dry Technol.* 22 (2004) 1403–1461.
<https://doi.org/10.1081/DRT-120038735>.
- [21] Malvern Panalytical, White paper - A Basic Guide to Particle Characterization Techniques, 2023.
<https://www.malvernpanalytical.com/en/learn/knowledge-center/whitepapers/wp120620basicguidepartchar> (accessed April 20, 2023).

Tables

Table 1: Coded variable levels and corresponding natural variable levels for the three studied factors. Also included are the calibration data for fines mass flow rate for tested conveyor frequencies and air flow rate for tested capacities with corresponding 95% confidence interval (CI).

| Coded variables | Natural variables | | | | |
|-----------------|----------------------|---|------------------------------------|--|------------------|
| | x_1 | x_2 | | x_3 | |
| | $T_{in} (^{\circ}C)$ | \dot{m}_{fines} | | $\dot{m}_{dry\ air}$ | |
| | Design variable (Hz) | Actual value \pm 95% CI ($kg \cdot h^{-1}$) | Design variable – Air capacity (%) | Actual value - $\dot{m}_{dry\ air} \pm$ 95% CI ($kg \cdot h^{-1}$) | |
| $-\alpha$ | 160 | 20 | 7.1 \pm 0.2 | 70 | 473.3 \pm 5.2 |
| -1 | 168 | 26 | 7.7 \pm 0.0 | 74 | 503.1 \pm 11.4 |
| 0 | 180 | 35 | 10.8 \pm 0.2 | 80 | 541.3 \pm 5.2 |
| 1 | 192 | 44 | 14.0 \pm 0.0 | 86 | 578.0 \pm 13.7 |
| α | 200 | 50 | 15.9 \pm 0.1 | 90 | 592.9 \pm 9.6 |

Table 2: Particle classes categorized according to specifically defined shape factors as calculated by the Morphology 4 image analysis software. Particles that did not belong to any of these three classes, were categorized as ‘other’ (N_o). The convex hull area is the area of the object if an imaginary “rubber band” is wrapped around the 2D projection. 2500 random examples of the three main classes can be found as gif under supplementary data.

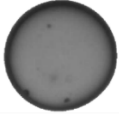


| <i>Particle class</i> | <i>High Sensitivity Circularity (HS)</i> $\left(\frac{\text{Perimeter}}{\text{Perimeter equiv. area circle}}\right)^2$ | <i>Solidity</i> $\frac{\text{Actual area}}{\text{Convex hull area}}$ | <i>Elongation</i> $1 - \frac{\text{width}}{\text{length}}$ | <i>Example particle with equivalent area circle (CE) diameter</i> |
|--|---|---|---|---|
| <i>Primary particles (N_{pp})</i> | ≥ 0.98 | > 0.6 | < 0.1 |  98.21 μm |
| <i>Partially coalesced particles (N_{pc})</i> | $0.98 > \dots \geq 0.8$ | > 0.6 | < 0.7 |  93.45 μm |
| <i>Agglomerated particles (N_{agg})</i> | < 0.8 | > 0.6 | < 0.7 |  117.92 μm |

Table 3: Experimental results following the CCD. Included are processing values (physical factor levels for x_1 , x_2 , and x_3 , the fines to spray F:S ratio on dry basis, and the heat supplied by the drying air) and experimental outcomes (agglomeration index AI, the number fraction of particles with different morphology, and the moisture content).

| CCD point | Block | T_{in} °C | m_{fines} kg·h ⁻¹ | m_{dry} air kg·h ⁻¹ | F:S | Q_{da} kJ·kg ⁻¹ | AI | N_{agg} | N_{pc} | N_{pp} | N_o | MC (%) |
|------------|-------|----------------|-----------------------------------|--|-------|---------------------------------|-------|-----------|----------|----------|-------|----------------|
| (-1,1,-1) | 1 | 168 | 14.0 | 515.4 | 1.640 | 5555 | 0.153 | 0.064 | 0.428 | 0.492 | 0.017 | 4.09 ± 0.43 |
| (-1,-1,1) | 1 | 168 | 7.7 | 589.7 | 0.905 | 6128 | 0.043 | 0.087 | 0.431 | 0.459 | 0.022 | 3.47 ± 0.31 |
| (0,0,0) | 1 | 180 | 10.8 | 540.5 | 1.272 | 6051 | 0.090 | 0.053 | 0.542 | 0.383 | 0.022 | 3.22 ± 0.38 |
| (0,0,0) | 1 | 180 | 10.8 | 545.9 | 1.272 | 6064 | 0.049 | 0.087 | 0.433 | 0.460 | 0.020 | 2.84 ± 0.08 |
| (1,-1,-1) | 1 | 192 | 7.7 | 512.7 | 0.905 | 6002 | 0.052 | 0.081 | 0.432 | 0.464 | 0.024 | 2.75 ± 0.23 |
| (1,1,1) | 1 | 192 | 14.0 | 571.7 | 1.647 | 6501 | 0.097 | 0.092 | 0.393 | 0.487 | 0.028 | 1.90 ± 0.27 |
| (-1,-1,-1) | 2 | 168 | 7.7 | 513.8 | 0.901 | 5609 | 0.061 | 0.105 | 0.444 | 0.430 | 0.021 | 4.14 ± 0.04 |
| (-1,1,1) | 2 | 168 | 14.0 | 592.5 | 1.640 | 6275 | 0.148 | 0.132 | 0.407 | 0.441 | 0.020 | 3.75 ± 0.03 |
| (0,0,0) | 2 | 180 | 10.8 | 534.8 | 1.272 | 6116 | 0.074 | 0.073 | 0.537 | 0.372 | 0.018 | 3.39 ± 0.00 |

| | | | | | | | | | | | | |
|----------|---|-----|------|-------|-------|------|-------|-------|-------|-------|-------|----------------|
| (0,0,0) | 2 | 180 | 10.8 | 522.6 | 1.266 | 5876 | 0.102 | 0.148 | 0.410 | 0.421 | 0.022 | 3.67 ± 0.11 |
| (1,1,-1) | 2 | 192 | 14.0 | 475.7 | 1.647 | 5800 | 0.164 | 0.102 | 0.475 | 0.404 | 0.019 | 3.48 ± 0.06 |
| (1,-1,1) | 2 | 192 | 7.7 | 545.1 | 0.901 | 6302 | 0.053 | 0.075 | 0.495 | 0.410 | 0.020 | 2.49 ± 0.02 |
| (-α,0,0) | 3 | 160 | 10.8 | 548.1 | 1.296 | 5708 | 0.074 | 0.185 | 0.429 | 0.363 | 0.021 | 3.71 ± 0.00 |
| (0,0,-α) | 3 | 180 | 10.8 | 478.9 | 1.284 | 5614 | 0.054 | 0.149 | 0.440 | 0.391 | 0.020 | 3.89 ± 0.00 |
| (0,-α,0) | 3 | 180 | 7.1 | 540.0 | 0.847 | 6125 | 0.046 | 0.090 | 0.444 | 0.445 | 0.021 | 3.34 ± 0.02 |
| (0,0,0) | 3 | 180 | 10.8 | 538.6 | 1.290 | 6054 | 0.058 | 0.115 | 0.453 | 0.415 | 0.017 | 3.20 ± 0.06 |
| (0,0,0) | 3 | 180 | 10.8 | 530.6 | 1.290 | 6148 | 0.047 | 0.107 | 0.427 | 0.448 | 0.019 | 3.16 ± 0.04 |
| (0,α,0) | 3 | 180 | 10.9 | 537.7 | 1.912 | 6122 | 0.115 | 0.178 | 0.400 | 0.401 | 0.021 | 3.13 ± 0.02 |
| (0,0,α) | 3 | 180 | 10.8 | 598.9 | 1.296 | 6625 | 0.037 | 0.174 | 0.426 | 0.377 | 0.023 | 2.25 ± 0.03 |
| (α,0,0) | 3 | 200 | 10.8 | 528.6 | 1.296 | 6567 | 0.042 | 0.158 | 0.399 | 0.420 | 0.024 | 2.44 ± 0.01 |
| (-α,0,0) | 4 | 160 | 10.8 | 558.2 | 1.254 | 5604 | 0.066 | 0.054 | 0.515 | 0.416 | 0.016 | 3.81 ± 0.30 |

Figures

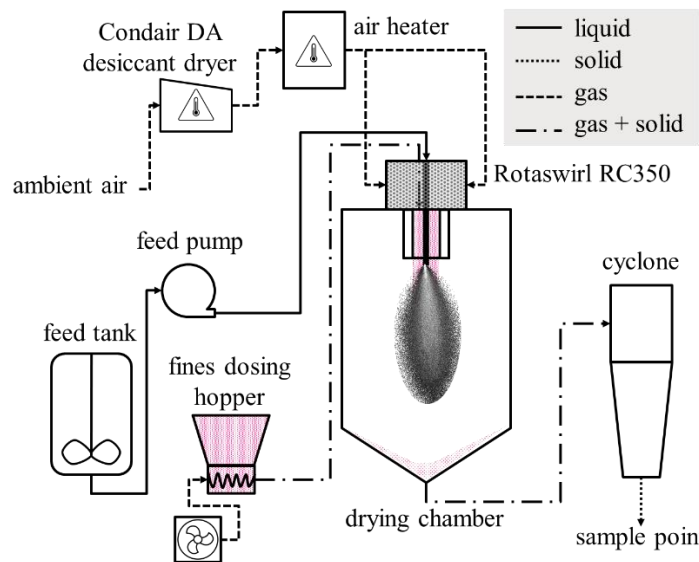


Figure 1: Schematic overview of the DW-350 pilot scale spray dryer, not to scale.



Figure 2: Schematic overview of the nozzle and inlet position of the fines, not to scale. Also pictured is the 25 cm extension of the inner/outer tubes.

Journal Pre-proof

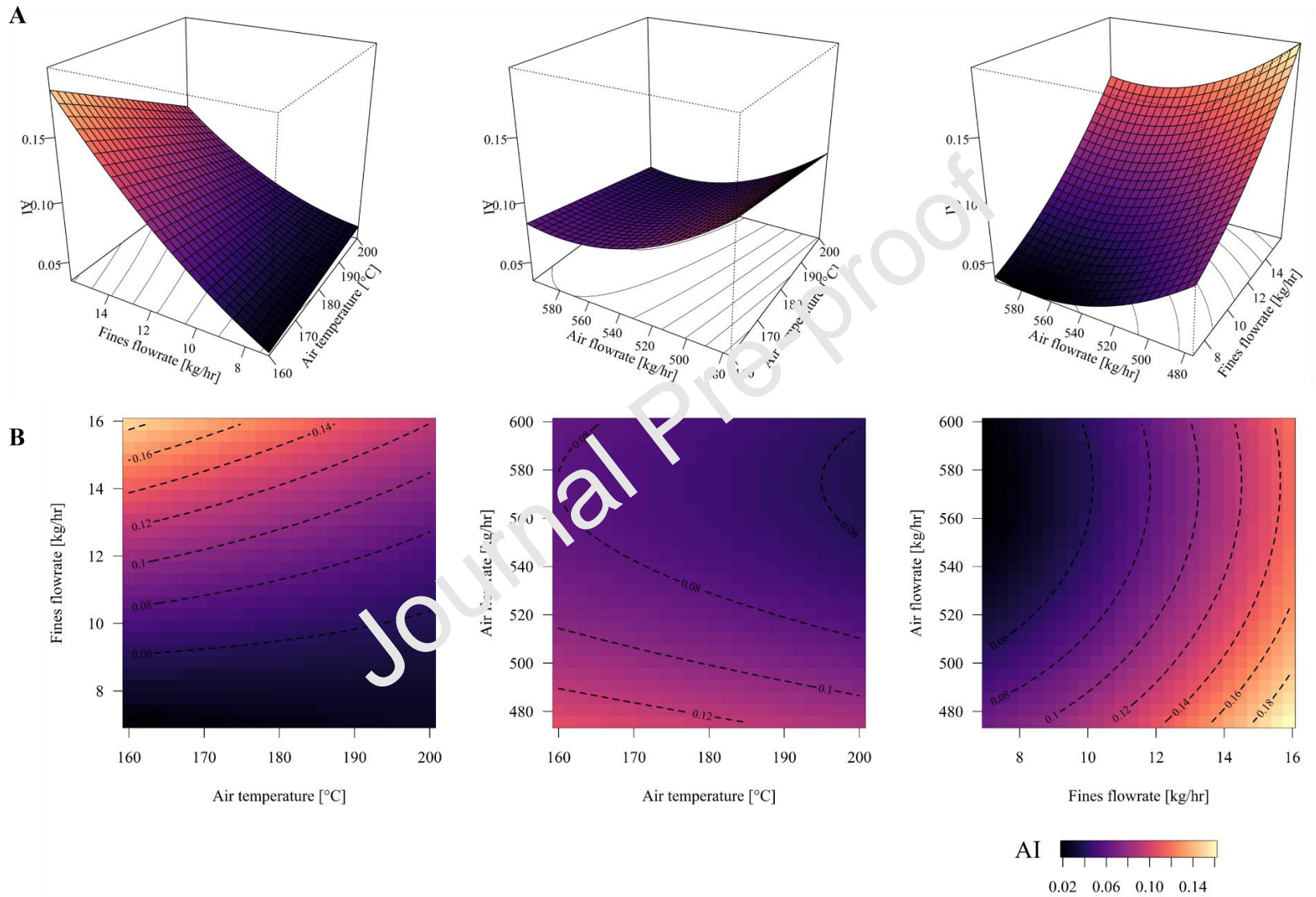


Figure 3: Agglomeration index (AI) response surface plots (A) and contour plots (B) for factor pairs, while the third factor is set at its midpoint.

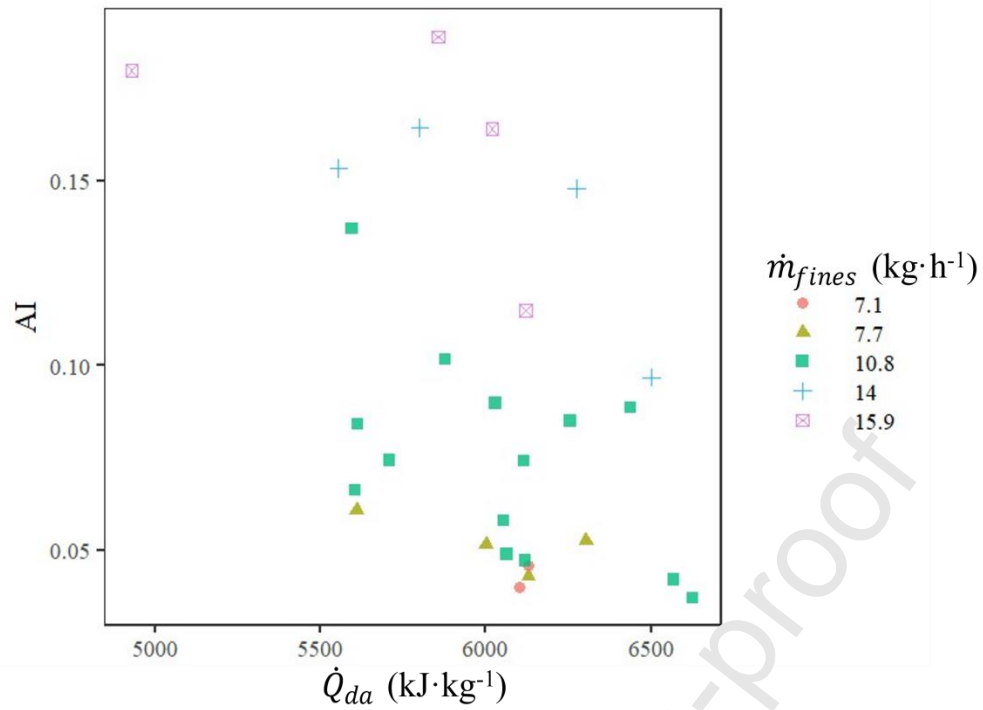


Figure 4: Agglomeration index (AI) as function of thermal energy per kg feed supplied by the drying air for different mass flowrates of fines.

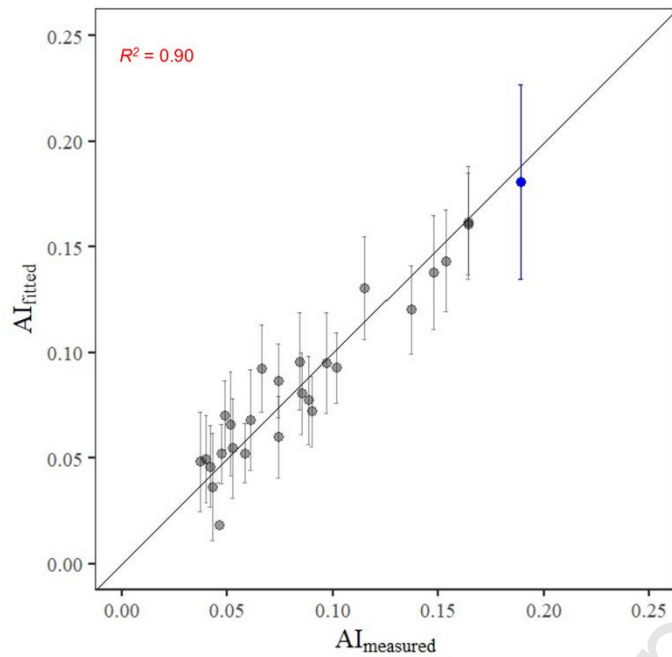


Figure 5: Fitted AI against measured AI values with a linear fit, corresponding R^2 value, and error bars signifying the 95% confidence intervals of fitted values. Grey points indicate CC conditions used to develop the model while the blue point (far right) is the test condition.

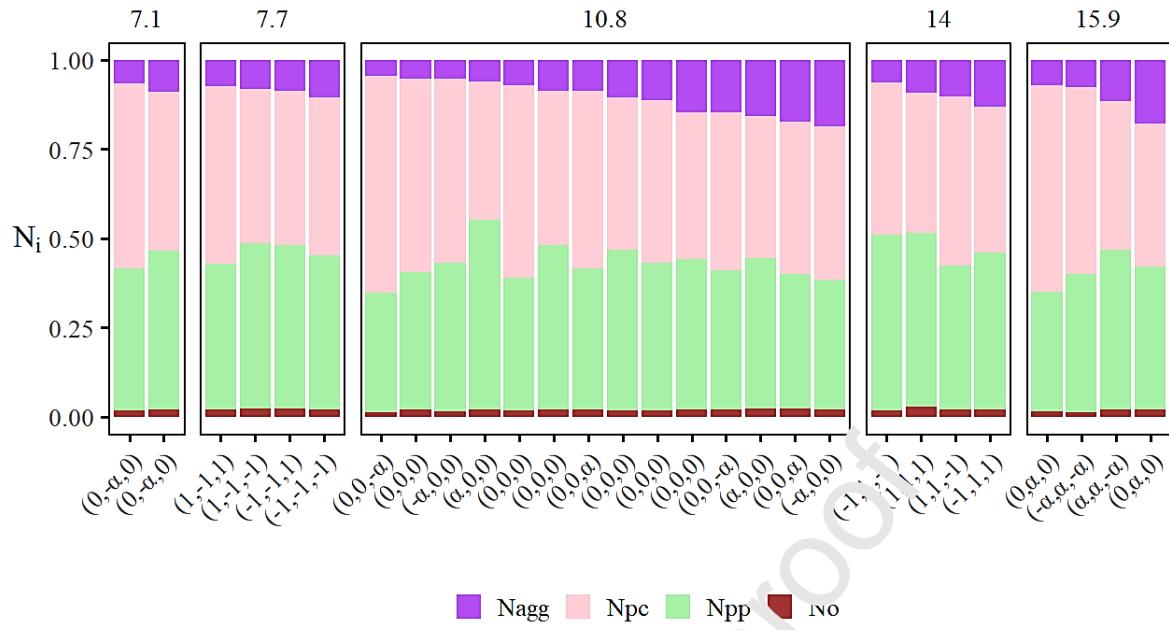


Figure 6: Particles categorized in classes per sample. The bars are grouped per fines mass flowrate ($\text{kg}\cdot\text{h}^{-1}$, indicated above plot) and ordered within each group by ascending N_{agg} .

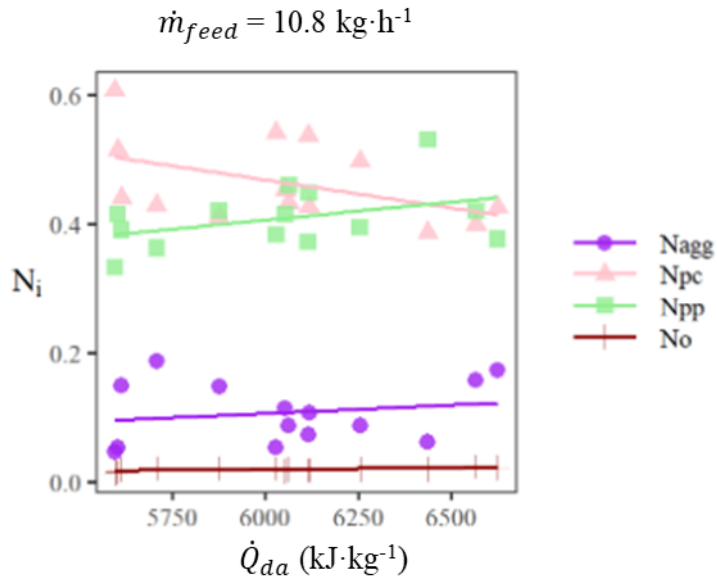


Figure 7: Fraction of particles in subclasses N_{agg} , N_{pc} , N_{pp} and N_o as a function of thermal energy per amount of feed (\dot{Q}_{da} (kW)) provided by the drying air for different fines mass flowrates. Lines are drawn to guide the eye.

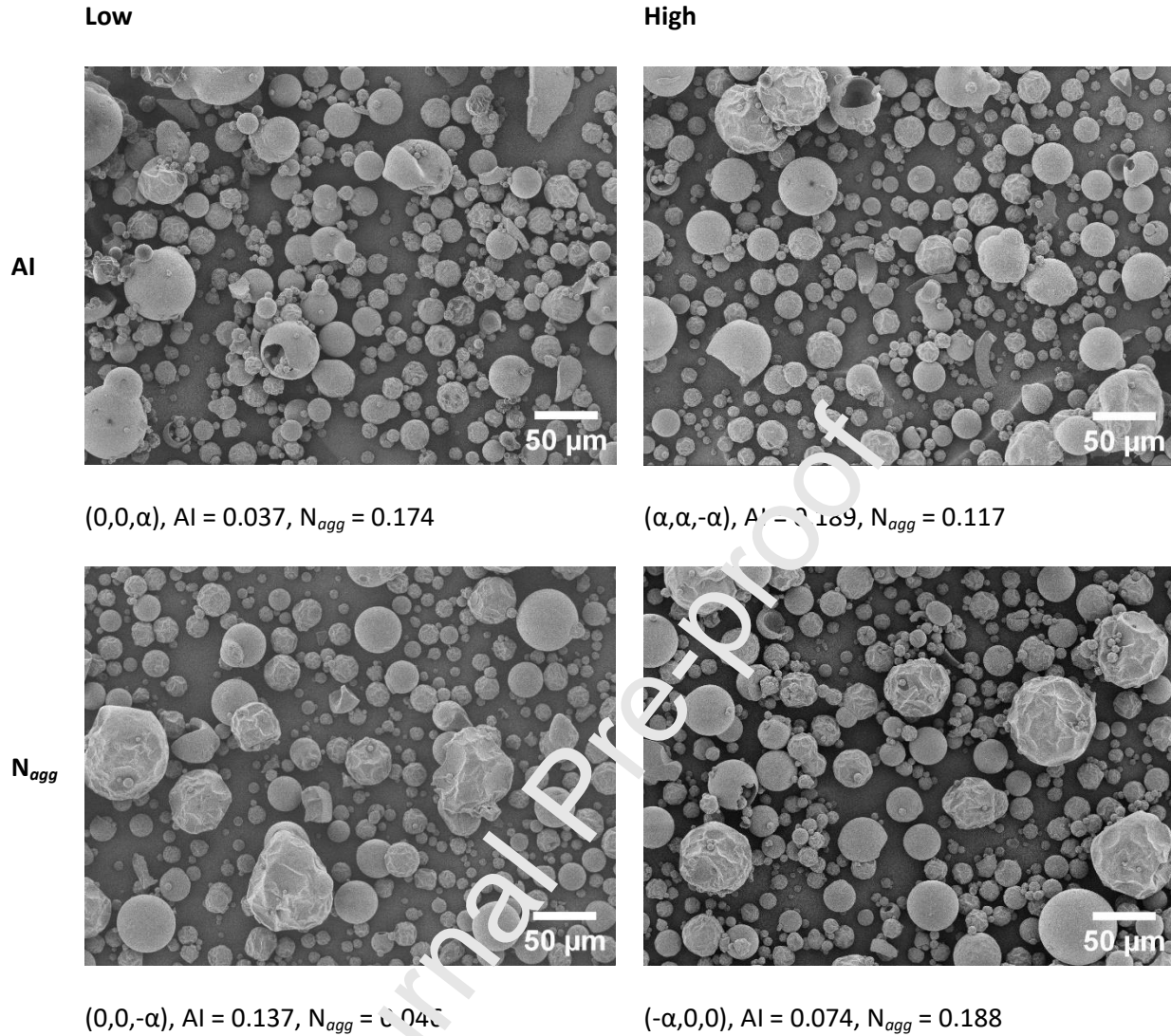


Figure 8: Particle morphology visualized by SEM. The depicted samples are those with the lowest and highest AI values and those with the lowest and highest N_{agg} values. All images were 300x enlarged.

8. Appendix

Table A. 1: Full CCD design organized by blocks showing treatment combinations with actual values for coded variables.

Factorial points are labelled (F), axial points (A), and center points (C).

| <i>Coded variables</i> | | | | |
|------------------------|----------------|-------------------------|-------------------------------|-------|
| | $T_{in} (x_1)$ | $\dot{m}_{fines} (x_2)$ | $\dot{m}_{drying\ air} (x_3)$ | Block |
| F | -1.01 | 1.00 | -0.71 | 1 |
| F | -1.01 | -0.98 | 1.32 | 1 |
| C | 0.00 | 0.00 | -0.02 | 1 |
| C | 0.00 | 0.00 | 0.12 | 1 |
| F | 1.01 | -0.98 | -1.03 | 1 |
| F | 1.01 | 1.00 | 0.83 | 1 |
| F | -1.01 | -0.98 | -0.75 | 2 |
| F | -1.01 | 1.00 | 1.40 | 2 |
| C | 0.00 | 0.00 | -0.18 | 2 |
| C | 0.00 | 0.00 | -0.51 | 2 |
| F | 1.01 | 1.00 | -1.79 | 2 |
| F | 1.01 | -0.98 | 0.10 | 2 |
| A | -1.68 | 0.00 | 0.19 | 3 |
| A | 0.00 | 0.00 | -1.70 | 3 |
| A | 0.00 | -1.16 | -0.04 | 3 |

| | | | | |
|---|-------|-------|-------|---|
| C | 0.00 | 0.00 | -0.07 | 3 |
| C | 0.00 | 0.00 | -0.05 | 3 |
| A | 0.00 | 1.61 | -0.10 | 3 |
| A | 0.00 | 0.00 | 1.57 | 3 |
| A | 1.68 | 0.00 | -0.35 | 3 |
| A | -1.68 | 0.00 | 0.46 | 3 |
| A | 0.00 | 0.00 | -1.42 | 4 |
| A | 0.00 | -1.16 | 0.31 | 4 |
| A | 0.00 | 1.61 | 0.28 | 4 |
| A | 0.00 | 0.00 | 1.23 | 4 |
| A | 1.68 | 0.00 | -0.15 | 4 |

Table A. 2: Parameter estimates for the AI model including significance level (*=0.05; **=0.01, ***=0).

| | Estimate | Std. Error | 95% CI (\pm) | t value | Pr(> t) | |
|--------------|----------|------------|------------------|---------|----------|-----|
| β_0 | 0.07172 | 0.00776 | 0.01645 | 9.25 | 8.1E-08 | *** |
| β_{D2} | 0.01272 | 0.00957 | 0.02030 | 1.28 | 2.2E-01 | |
| β_{D3} | -0.02041 | 0.00887 | 0.01879 | -2.30 | 3.5E-02 | * |
| β_{D4} | 0.01440 | 0.00943 | 0.01998 | 1.53 | 1.5E-01 | |
| β_1 | -0.00648 | 0.00384 | 0.00814 | -1.69 | 1.1E-01 | |
| β_2 | 0.03689 | 0.00441 | 0.00936 | 8.36 | 3.1E-07 | *** |
| β_3 | -0.01357 | 0.00394 | 0.00835 | -3.45 | 3.3E-03 | ** |

| | | | | | | |
|--------------|----------|---------|---------|-------|---------|---|
| β_{12} | -0.00779 | 0.00589 | 0.01249 | -1.32 | 2.0E-01 | |
| β_{22} | 0.00712 | 0.00449 | 0.00951 | 1.59 | 1.3E-01 | |
| β_{33} | 0.00739 | 0.00341 | 0.00722 | 2.17 | 4.5E-02 | * |

Table A. 3: Parameter estimates for N_{agg} model including significance level ($\circ = 0.1$; $*$ = 0.05; $*** = 0$).

| | <i>Estimate</i> | <i>Std. Error</i> | <i>95% CI (\pm)</i> | <i>t value</i> | <i>Pr(> t)</i> | |
|--------------|-----------------|-------------------|----------------------------------|----------------|--------------------|---------|
| β_0 | 0.07673 | 0.01038 | 0.02165 | 7.39 | 3.9E-07 | *** |
| β_{D2} | 0.03122 | 0.01482 | 0.03091 | 2.11 | 1.8E-02 | * |
| β_{D3} | 0.06796 | 0.01374 | 0.02867 | 4.94 | 7.8E-05 | *** |
| β_{D4} | -0.01378 | 0.01467 | 0.03060 | -0.94 | 3.6E-01 | |
| β_2 | 0.01091 | 0.00642 | 0.01310 | 1.70 | 1.0E-01 | \circ |
| β_3 | 0.00821 | 0.00585 | 0.01220 | 1.40 | 1.8E-01 | |

Author CRediT statement

- Anneloes van Boven: Conceptualization, investigation, methodology, writing – original draft
- Santiago Calderon Novoa: Investigation, methodology, formal analysis, writing – original draft
- Reinhard Kohlus: Conceptualization, funding acquisition, supervision, writing – review & editing
- Maarten Schutyser: Conceptualization, funding acquisition, supervision, writing – review & editing

Journal Pre-proof

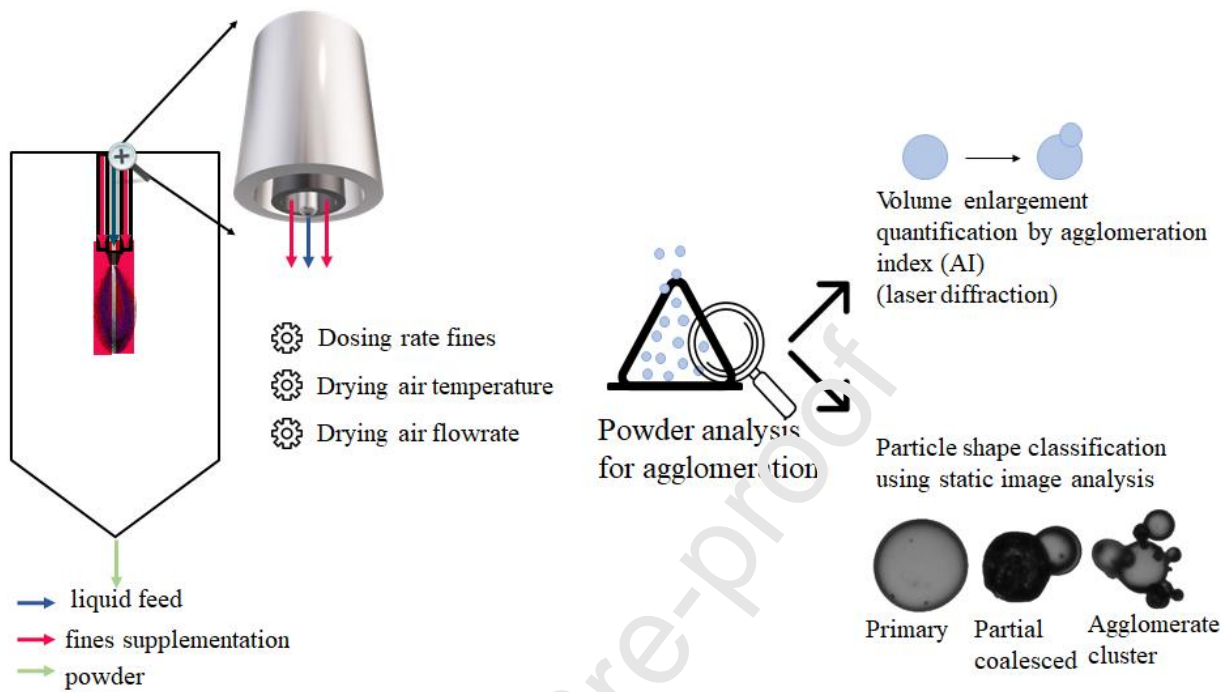
Declaration of Interest Statement

This work is an Institute for Sustainable Process Technology (ISPT) project, i.e. StAggloP (Project number: DR-50-15). Partners in this project are Corbion, Danone, DSM, FrieslandCampina, University of Hohenheim, Wageningen University & Research, and ISPT. This project is co-funded with subsidy from the Topsector Energy by the Dutch Ministry of Economic Affairs and Climate Policy.

None of the authors has any conflict of interest to declare.

Journal Pre-proof

Graphical Abstract



Highlights:

- Agglomeration increases with a higher collision frequency in the nozzle zone
- The dosing rate of fine powder impacted agglomeration the most
- Higher drying rates reduced nozzle zone agglomeration
- The onset of nozzle zone agglomeration can best be studied using image analysis

Journal Pre-proof